Supporting Information for

Cyanobacterial aldehyde deformylase oxygenation of aldehydes yields n-1 aldehydes and alcohols in addition to alkanes

*Kelly G. Aukema[†] Thomas M. Makris[‡§], Sebastian A. Stoian[¶£], Jack E. Richman[†], Eckard Münck[¶], John D. Lipscomb[‡], Lawrence P. Wackett[†‡]**

*wacke003@umn.edu

[†]BioTechnology Institute University of Minnesota, St. Paul, Minnesota 55108 and [‡]Department of Biochemistry, Molecular Biology and Biophysics, University of Minnesota, Minneapolis, Minnesota 55455, and [¶]Department of Chemistry, Carnegie Mellon University, Pittsburgh, Pennsylvania 15213 [§]Current address: Department of Chemistry and Biochemistry, University of South Carolina, 631 Sumter Street, Columbia, SC 29208 [£]Current address: National High Magnetic Field Laboratory, Florida State University, 1800 E. Paul Dirac Drive, Tallahassee, FL 32310–3706

Oxygen Scavenged ADO Reactions. All components of the ADO reaction were degassed with alternating argon and vacuum on a Schlenk line and moved into an anaerobic chamber. 10 μM of purified 2,3 homoprotocatechuate dioxygenase and 250 μM homoprotocatechuate were added to a standard ADO reaction with 500 μM dodecanal and 30 μM ADO. The formation of the extradiol cleavage product, yellow in color, confirmed the presence of trace O_2 in the reaction. The dioxygenase was allowed to scavenge oxygen for 10 minutes, inside the anaerobic chamber prior to NADH initiation of the ADO reaction.

HPLC-MS Detection of Formaldehyde and Formate. The aqueous layer of an extracted aldehyde deformylase reaction ([^{13}C]-nonanal, 100 μM ADO, NADPH/ferredoxin) was collected and derivatized for formate or formaldehyde detection by ESI LC-MS on a ThermoFisher LCQ Classic. Derivatized samples were separated on an Agilent Eclipse XDB-C18 column and eluted with a gradient of 2-100% acetonitrile over 20 minutes. Formate and a propionate standard were derivatized with 2-nitrophenyl hydrazine for detection by negative mode ESI HPLC-MS according to the methods of Warui *et al*.[1] Formaldehyde was derivatized with acetylacetone to yield diacetyldihydrolutidine[2] and analyzed by positive mode HPLC-MS (ESI, m^+/z 194^+ [M^+H^+] or 195^+ for [^{12}C]- or [^{13}C]-formaldehyde, respectively) according to the methods of Numazawa *et al.*[3]

Myoglobin-Binding Assay for Carbon Monoxide Detection. Using the methods of Wauri *et al*., standard 100 μM ADO reactions with NADH/phenazine were carried out with 500 μM nonanal in septum sealed cuvettes.[1] After ten minutes, fresh myoglobin (equine) and sodium dithionite were mixed together and injected into the cuvettes at a final concentration of 4 μM and 20 mM respectively. Visible spectra were collected from 400-500 nm on a Beckman spectrophotometer. Subsequently, carbon monoxide saturated water at 0˚C (~1.2 mM) was added to reaction mixtures at 12 μM final concentration carbon monoxide, and visible spectra were collected and analyzed for the appearance of the Soret shift at 425 nm**.**

Synthesis of ^{13}C-Labeled Aldehydes and Alcohol. [1-^{13}C]- Octanoic acid and [1,2-^{13}C] - octanoic acid were purchased from Sigma. [1-^{13}C]-Nonanoic acid was synthesized using standard methods from commercially available octyl magnesium bromide (Sigma). Labeled aldehydes were made from the labeled acids by conversion to acid chloride with thionyl chloride using standard methods followed by catalytic reduction with tributyltin hydride and a palladium

catalyst.[4] Products were confirmed by ^{13}C-NMR analysis (Varian 400 MHz) (Supporting Information Figure S4 and S6). [1-^{13}C]-Nonanoic acid was converted to [1-^{13}C]-1-nonanol with borane-tetrahydrofuran using the methods of Kende and Fludzinski.[5]

EPR and Mössbauer Methods. EPR spectra were measured using a Bruker Elexsys E-500 spectrometer equipped with a Bruker dual mode cavity and Oxford ESR 910 liquid helium cryostat. The software package SpinCount (M.P. Hendrich, Carnegie Mellon University) was used to analyze the spectra. The Mössbauer spectrometer was of the constant acceleration type. The measurements were performed in a superconducting magnet system (Janis Research Company SuperVariTemp dewar and an American Magnetics 8.0 T magnet with quick null). The source, 60 mCi ^{57}Co diffused into a rhodium foil, was mounted on a vertical suspension system inserted into the dewar; the Mössbauer transducer was mounted on top of the dewar. Samples were filled into Delrin cups, frozen in liquid nitrogen, and then mounted into an aluminum holder assembly. The latter was provided with a heater wire and a calibrated Cernox temperature sensor (Lakeshore Cryotronix). For measurements at 4.2 K the sample chamber was flooded with liquid helium. For higher temperatures helium was admitted through a capillary and the flow of helium was controlled by a needle valve. Under these conditions the sample was exposed to a gas stream. Between 15 K and 200 K the temperature was known to within ±1 K; the stability was better than 0.1 K over a period of 24 hours. The velocity was calibrated by using an Fe metal absorber at 298 K or 4.2 K. Spectra were analyzed using the WMOSS (SEE Co, Edina, MN, USA) software package.

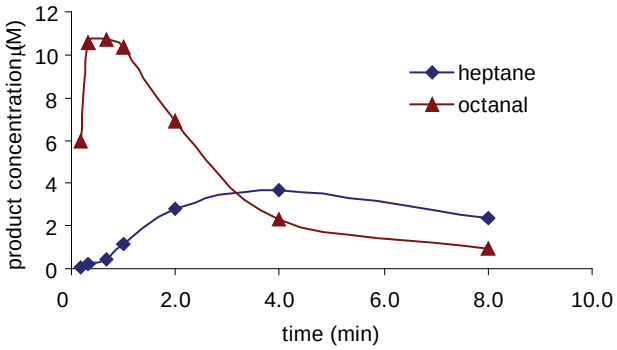

Figure S1. Heptane and octanal concentration as a function of time during a 100 μM ADO reaction with nonanal as analyzed by GC/MS. Same samples as in Figure 1C.

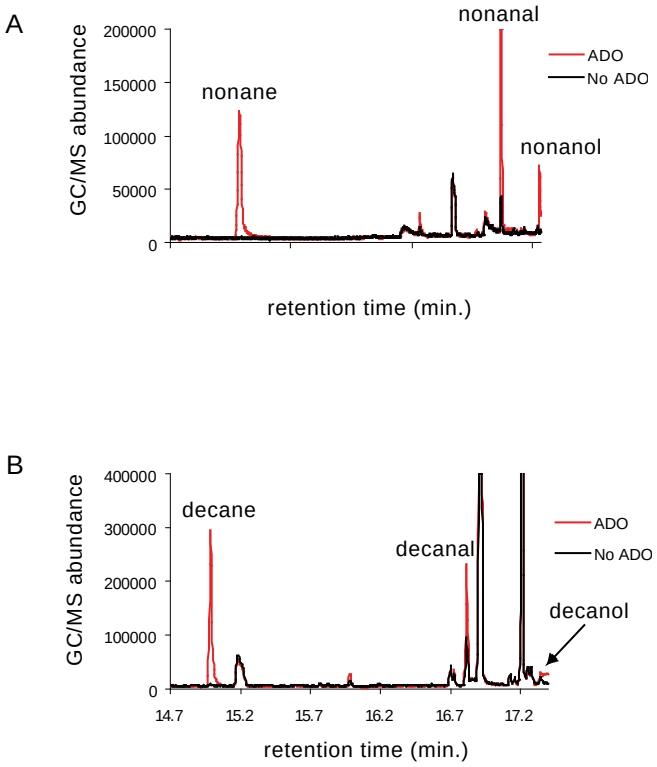

Figure S2. GC/MS chromatogram of ADO reaction mixtures with (red) and without (black) 30μM ADO incubated with A) 500μM decanal or B) 500μM undecanal.

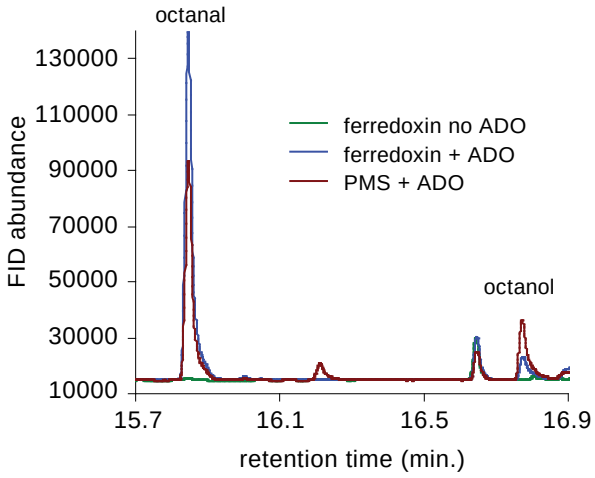

Figure S3. GC/FID chromatogram of ADO reaction with nonanal using spinach ferredoxin or phenazine (PMS) as electron shuttle.

^{13}C-NMR $CDCl_3$

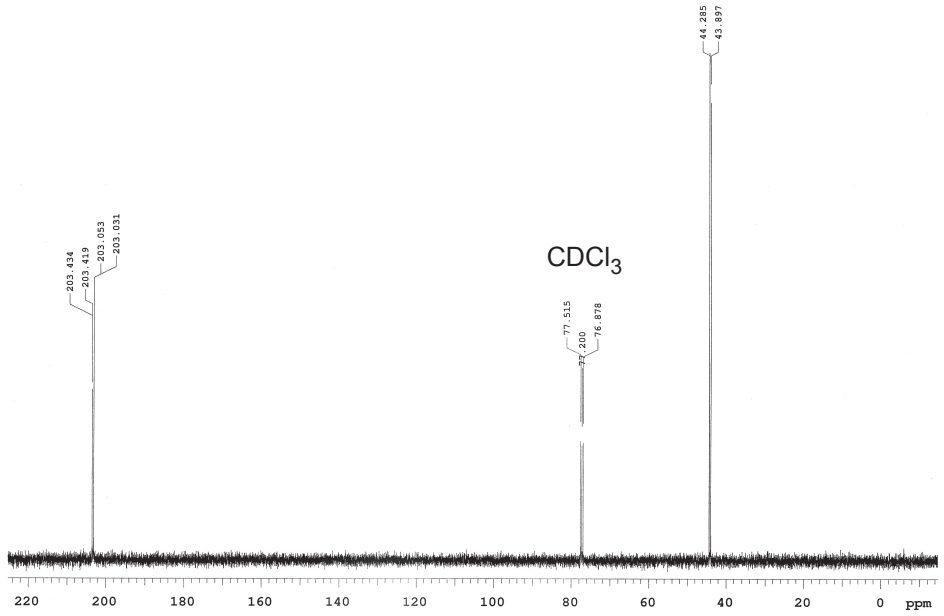

^{1}H-NMR $CDCl_3$

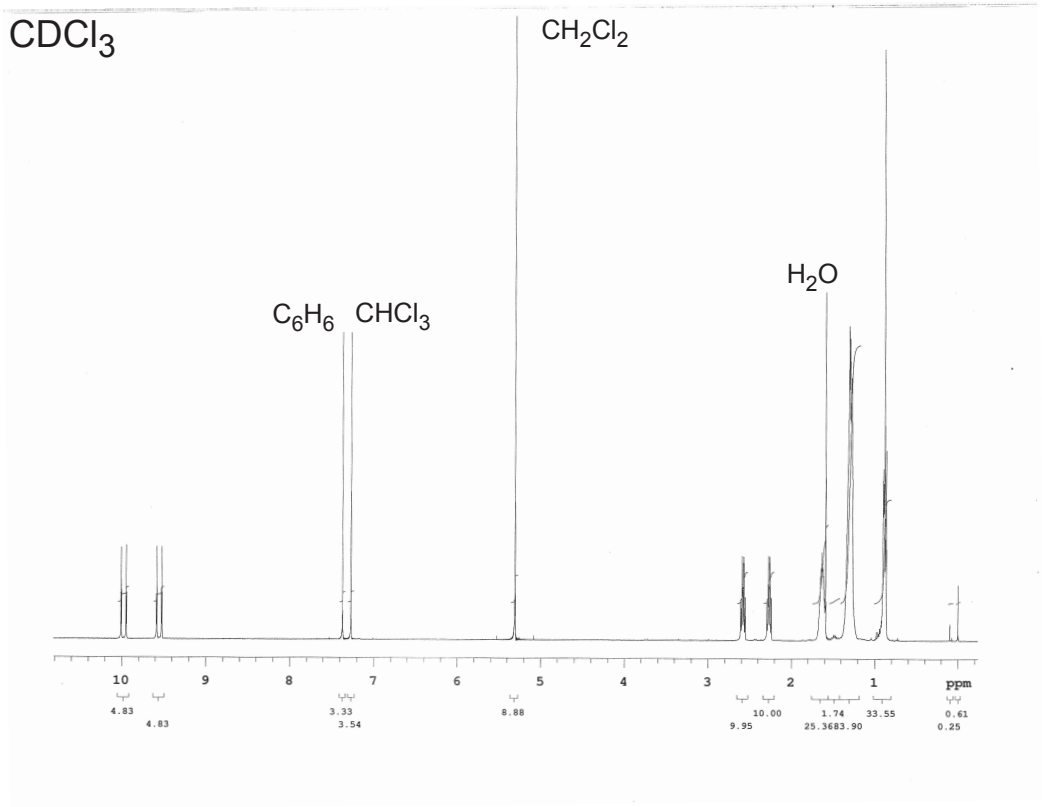

Figure S4. ^{13}C-NMR and ^{1}H-NMR of synthesized [1,2-^{13}C]-octanal. Solvents and contaminants are labeled.

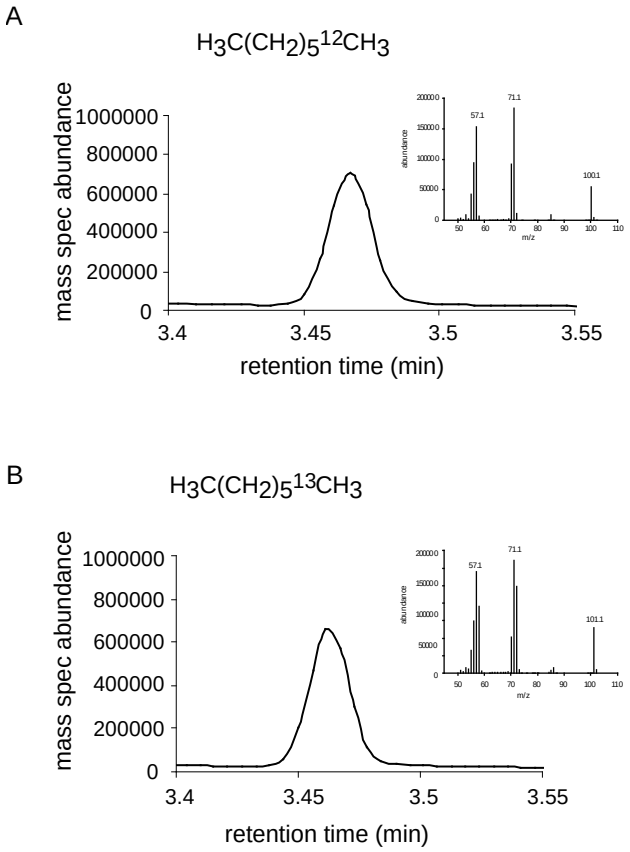

Figure S5. GC/MS chromatogram and mass spectrum (inset) of heptane product of AD reaction with A) Octanal and B) [1,2-^{13}C]-Octanal.

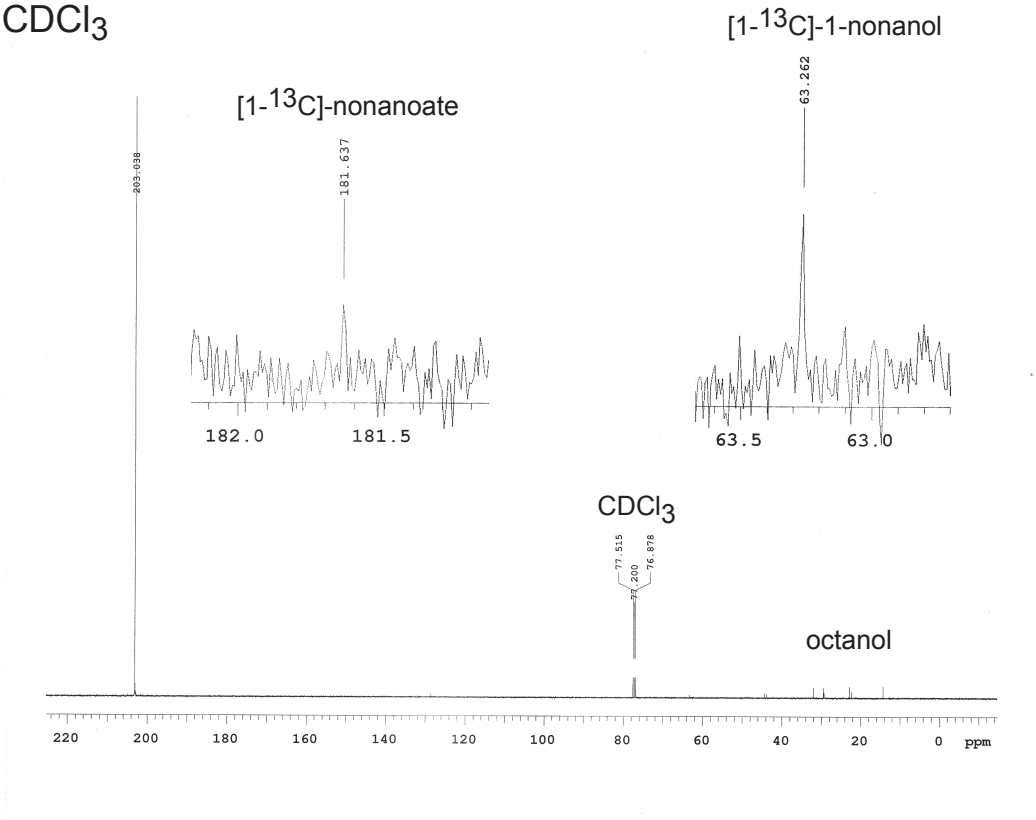

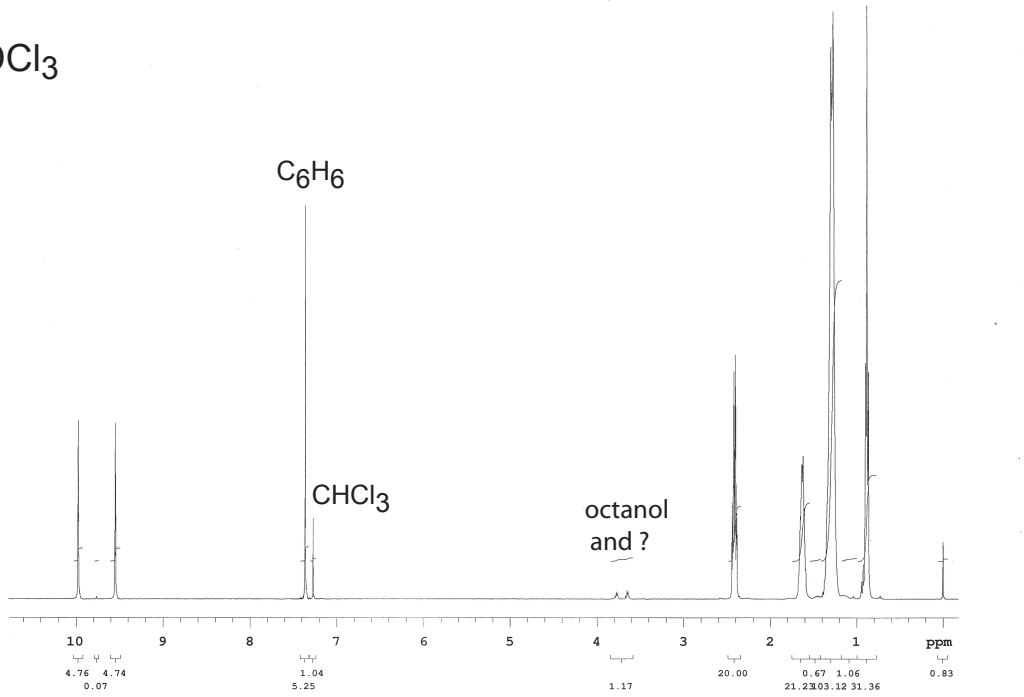

Figure S6. ^{13}C-NMR and ^{1}H-NMR of synthesized [1-^{13}C]-nonanal. Solvents and contaminants are labeled. Expanded views of [1-^{13}C]-nonanoate and [1-^{13}C]-1-nonanol peaks are inset.

Table S1.

	194^{+} / 195^{+a}
[1-^{13}C]-nonanal	0.12
[1-^{13}C]-nonanal without NADH	0.10
[1-^{12}C]-nonanal	0.13
[1-^{13}C]-nonanal + 100μM [^{13}C]-formaldehyde	2.50
[1-^{13}C]-nonanal + 50μM [^{13}C]-formaldehyde	1.35
[1-^{13}C]-nonanal + 30μM [^{13}C]-formaldehyde	0.85

[a] ratio of 194^{+} peak area to 195^{+} peak area as determined by HPLC-ESI/MS

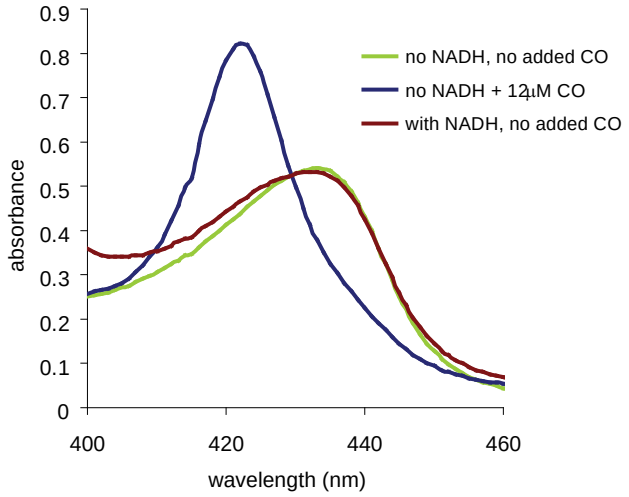

Figure S7. Detection of CO via visible absorbance spectra of myoglobin. Two standard 100 μM ADO reactions with phenazine, one with (red) and one without (green) NADH were incubated with 500 μM nonanal for ten minutes before the addition of myoglobin and dithionite at a final concentration of 6 μM and 20 μM, respectively. CO was added at 12 μM final to the reaction mixture without NADH (blue).

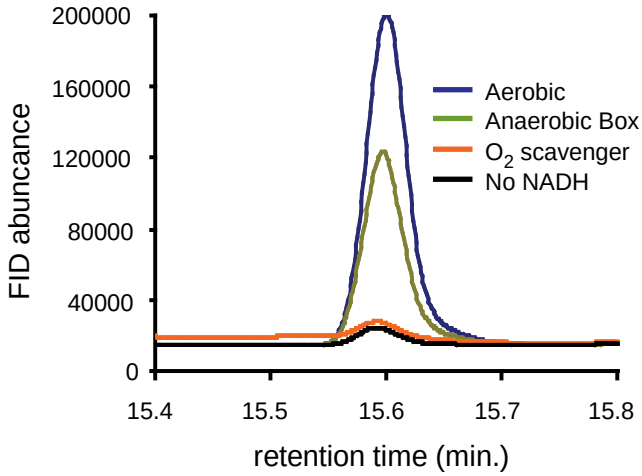

Figure S8. GC/FID chromatograms of ADO reaction mixtures with dodecanal. Undecane peak shown. Reactions were carried out under the following conditions: aerobic (blue), in an anaerobic chamber with (red) and without oxygen scavenging system (green), and without NADH (black).

Comments on the Analysis of the Mössbauer and EPR Spectra. In the following we address some points regarding the analysis of the Mössbauer and EPR spectra of reduced ADO. For some readers it might be useful to consult the review by Münck *et al*. that specifically addresses the benefits of undertaking a combined integer spin EPR and Mössbauer spectroscopic analysis.[6]

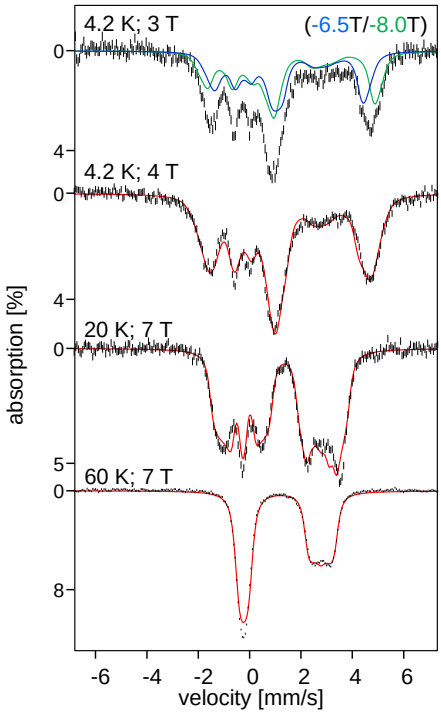

Figure S9. Selected Mössbauer spectra of diferrous ADO recorded in applied fields and at the temperatures indicated. Spectra were recorded on the same sample as those of Figure 7. For the top spectrum (4.2 K, 3 T), the blue and green curves shows the simulated spectra of the individual iron site for which A_z = -6.5 T and -8.0 T, respectively. For the lower three spectra the solid red lines represent simulations obtained using eqs 1-4 and the parameters of Table 2 of the main text.

Figure S9 shows Mössbauer spectra not presented in the main text. As described in the main text, the integer spin EPR feature of the diiron cluster results from a transition between two closely-spaced spin states, labeled $|2^{up}>$ and $|2^{down}>$. In zero field, these states have an energy separation of $\Delta = \Delta_{1,2}^2/8J$, with $\Delta_{1,2} = 3(E/D)_{1,2}^2 D_{1,2}$, where $(E/D)_{1,2}$ stands for $(E/D)_1 = (E/D)_2$. The expressions for Δ and $\Delta_{1,2}$ are second-order perturbation expressions; the Δ values quoted in the main text are based on diagonalizing the entire Hamiltonian of eq 2 and have slightly different numerical values as those obtained from the second-order expressions. For $D_{1,2} < 0$ the $|2^{up}\rangle$ and $|2^{down}\rangle$ states of Figure S10 are derived from the $m_1 = \pm 2$ and $m_2 = \pm 2$ levels; m_1 and m_2 are the magnetic quantum numbers of site 1 and 2, respectively (we note that the two states also include a small admixture of $m_{1,2} = 0$ states; this admixture is responsible for the splittings $\Delta_{1,2}$); details are given in Hendrich *et al*.1989 and Hendrich *et al*. 1990.[7,8] The two states have only non-zero matrix elements with the *z*-components of the spin operators, i.e. $\langle 2^{\mathrm{down}} | \hat{S}_{zi} | 2^{\mathrm{down}} \rangle \neq 0$ where the index $i = 1, 2$ labels the two sites. The fact that only $\hat{S}_{z1}$ and $\hat{S}_{z2}$ have non-vanishing matrix elements implies that an EPR transition is observed between the two states when the magnetic component of the microwave field, B_{osc}, is along *z*. Furthermore, a static field **B**, also along *z*, mixes the $|2^{up}\rangle$ and $|2^{down}\rangle$ states generating finite expectation values $\langle \hat{S}_{z1} \rangle$ and $\langle \hat{S}_{z2} \rangle$ of the electronic spin along *z* while the corresponding *x* and *y* components are small for B < 3 T. Thus, the electronic ground state is magnetically uniaxial along *z*. (We do not yet know how *z* is related to the direction of the internuclear Fe – Fe direction of the diiron cluster.) A graph $\langle \hat{S}_{x,y,z} \rangle$ of site 1 *vs.* applied field, B, for the $|2^{down}\rangle$ state is shown in Figure S11; $\langle \hat{S}_{x,y,z\,1} \rangle = \langle 2^{down} | \hat{S}_{x,y,z\,1} | 2^{down} \rangle$. The mixing of the two states produces sizable internal magnetic fields at the ^{57}Fe nuclei through the magnetic hyperfine term, yielding $B_{int,z1} =$

$-\langle\hat{S}_{z1}\rangle A_{z1}/g_n\beta_n$. $\langle\hat{S}_{z1}\rangle$ follows a "magnetization" curve that saturates at $\langle\hat{S}_{z1}\rangle = -2$.The same curve applies for site 2. By recording spectra at 4.2 K for variable applied fields we obtain A_{z1} (and A_{z2}) from the Mössbauer spectra, and by additionally probing the expectation value of the electronic spin as a function of temperature we obtain the zero-field splittings of the two Fe sites. As a final comment, by virtue of the electronic properties dictated by the negative *D*-values, only the *z* component, J_z, of the exchange coupling *J* matters, i.e. we could have written $\hat{\mathrm{H}}_{exch} = J_z\hat{S}_{z1}\cdot\hat{S}_{z2}$ rather than $\hat{\mathrm{H}}_{exch} = J\hat{\mathbf{S}}_1\cdot\hat{\mathbf{S}}_2$ for the exchange term.

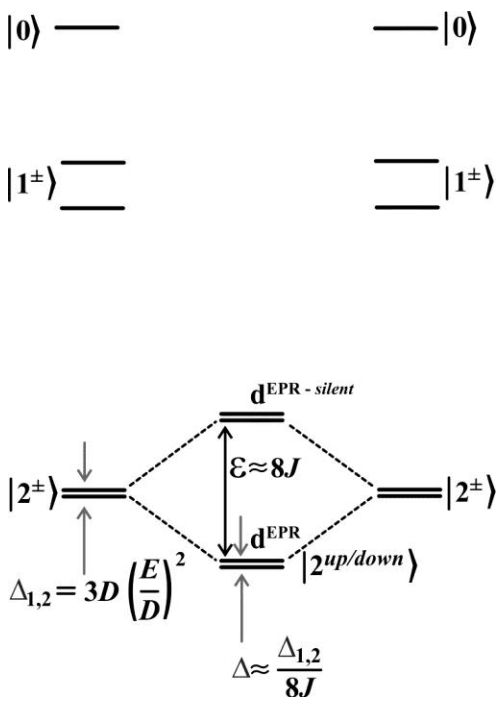

Figure S10. Spin levels of diferrous ADO plotted in the limit of weak ferromagnetic exchange coupling, i.e. $|J|$ << zero-field splittings. It is assumed that the zero-field splitting tensors of the two sites are equal and parallel, and that $D_1 = D_2 < 0$. The exchange splitting is shown only for

the $|2^{\pm}\rangle$ states. The states labeled $|2^{up}\rangle$ and $|2^{down}\rangle$ designate the members of the EPR-active doublet. At 4.2 K and for 2.0 T < B < 5.0 T only the $|2^{down}\rangle$ state (the spin-down state) is appreciably populated at 4.2 K. The doublet at energy $\varepsilon \approx 8J$ produced the quadrupole doublet generated by forming the difference spectrum "2 K minus 4.2 K" in Figure S12.

The presence of an "easy axis" of magnetization along *z* implies that the 4.2 K spectra, for B < 5 T, are essentially sensitive mainly to A_z and to the orientation of $B_{int,z}$ relative to the EFG tensor. For larger applied fields the increasing $\langle \hat{S}_{xi} \rangle$ and $\langle \hat{S}_{yi} \rangle$ components combine with A_x and A_y to produce large hyperfine fields in the *xy* plane, e. g. $B_{int,x}$ = -29.6 T and $B_{int,y}$ = -13 T for B = 7.0 T. The values of $\langle \hat{S}_x \rangle$ and $\langle \hat{S}_y \rangle$ near B = 7.0 T depend on E/D, and since we obtained a good estimate for A_x and A_y from the 120 K and 140 K spectra, the 4.2 K spectra give us an estimate of *E*/*D*.

Next, we consider the 7.0 T spectra recorded at T = 120 K and 140 K. For this temperature and applied field the spectra are independent of the exchange coupling constant *J*, and the zero-field splitting parameters D_i and $(E/D)_i$ influence the spectra only in a very minor way (and besides, these parameters are known reasonably well from the evaluation of the low temperature data). Above T = 100 K the thermal expectation values of the electronic spins are in the regime where the Curie law applies and the effective magnetic field acting at the ^{57}Fe nucleus along *j* = *x, y, z* is given by $\mathbf{B}_{eff} = \mathbf{B} + \mathbf{B}_{int}$ with $\mathbf{B}_{int,j} \approx \left(g_j \beta B_j / 3kT\right) A_j S(S+1)$, , where k is the Boltzmann constant and $S = 2$.[6] We have dropped the site index because the two iron sites are essentially equivalent and can be treated like mononuclear sites. $\mathbf{B}_{eff}$ is smaller than **B** because the components of the magnetic hyperfine tensors are negative. Our spectral simulation show that $\Delta E_Q > 0$ and suggest an asymmetry parameter $\eta \approx 0.7$, implying that the splitting of the high-

energy (right) feature of the 120 K and 140 K spectra depends on $B_{int,z}$ while that of the low-energy feature depends mainly on $B_{int,x}$ and $B_{int,y.}$ By using the A_z values obtained from the 4.2 K data we can fit the 120 K and 140 K spectra to obtain an estimate for g_z. This procedure yielded $2.0 < g_z < 2.30$, a constraint that can be used for the EPR simulations. A better constraint for g_z, however, may be obtained from the following consideration.

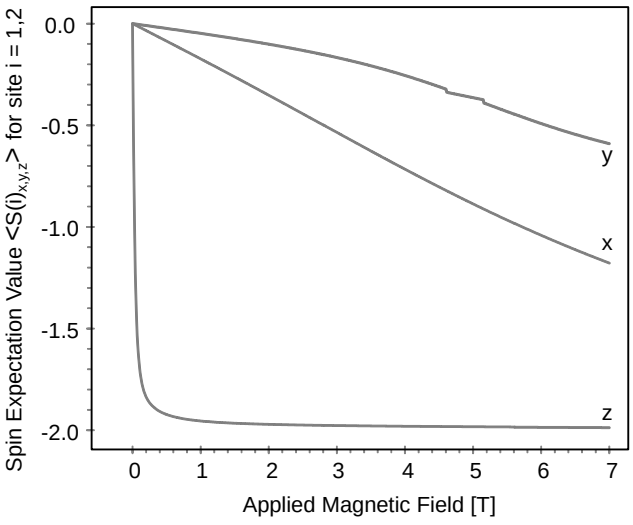

Figure S11. Graph of the expectation values $<S_{x,y,z}(i)>$ for site i = 1, 2 for the $|2^{down}>$ state as a function of the applied field B. $<S_j>$ is calculated with the field along direction i.

The magnetic hyperfine tensor components of the two Fe sites are approximately $A_{x,y,z}/g_n\beta_n \approx -(25, 22, 6.5/8)\mathrm{T}$; see Table 2 of the main text. These parameters can be used to obtain to constrain g_z by the following argument. Simplifying by assuming that the A - tensor is axial, the A - values would be those of a d_{xy} orbital for which we can write for the z component of the A-tensor the expression (see Fox *et al.*).[9]

(1)

Here P ≈ 61 T is a scaling constant appropriate for the present type of Fe^{II} site.[10-13] Pκ gives the Fermi contact contribution to A_z. Most frequently researchers use κ = 0.35. These values of P and κ are appropriate here as they produce almost exactly the Fermi contact contribution (-21.4 T) of the Fe^{II} site in the mixed-valence $Fe^{III}Fe^{II}$ form of MMOH.[9] The term P/7 = (61/7) T = +8.7 T gives the spin-dipolar contribution to A_z. Together, the Fermi contact and spin-dipolar contribution then yield -21.4 T + 8.7 T = -12.7 T. Given that the A_z of ADO is ≈ -7 T, we estimate $P(g_z-2) \approx +5.7$ T, which suggests $g_z \approx 2.09$.

We wish to comment briefly on the equivalence of the two iron sites of reduced ADO. As testified by the zero field spectrum of Figure 7, $\Delta E_Q(1) = \Delta E_Q(2)$ and $\delta(1) = \delta(2)$. Within our resolution all parameters except A_z are the same. A_{z1} must differ from A_{z2} for the following reason. Consider the 3.0 T spectrum of Figure S9. As shown in Figure S11, the system is roughly uniaxial up to fields of approximately 3 T. Under these conditions each site produces a 6-line spectrum with generally sharp absorption lines (unless A_z or $\langle S_z \rangle$ are distributed by heterogeneities). The blue line in 3.0 T spectrum of Figure S9 is a simulation for site 1. As can be seen the rightmost line of the experimental data is much broader and therefore must accommodate two slightly displaced lines (the blue and the green lines), i.e. the A_z values of the sites differ.

Table 2 of the main text shows that the $A_z/g_n\beta_n$ values of sites 1 and 2 differ by 1.5 T. Consequently, we may wonder what differences between the two sites account for the variation in A_z. It is very unlikely that the Fermi contact term differs between the two sites, and the spin-dipolar term, which is proportional to the valence part of the EFG, is expected to be the same for both sites as their the quadrupole interactions are the same. This leaves us with the orbital term

P(g_z-2) as the likely source. The reader may note that a even fairly small difference g_{z1} - g_{z2} = 0.025 would change the orbital contribution to A_z to account for the observed differences.

The Exchange Coupling in ADO is Small and Ferromagnetic. We have various lines of evidence that the exchange coupling is ferromagnetic. The most direct evidence can be obtained from the 0.3 T spectra of Figure S12 which were recorded at 4.2 K and 2 K. Consider again the diagrams of Figure S10 and S11. For ferromagnetic coupling the two levels constituting the ground doublet (states $|2^{up}>$ and $|2^{down}>$) produce sizable spin expectation values even in weak applied magnetic fields. In contrast, the first excited doublet at energy $\varepsilon \approx 8J$, labeled $d^{EPR\text{-}silent}$, produces only very small $<S_i>$ and therefore a small B_{int}. Its Mössbauer spectrum would consist of a broadened quadrupole doublet at B = 0.3 T, with absorption lines at -0.25 mm/s and + 2.85 mm/s Doppler velocity. At 4.2 K the two levels of excited spin doublet are populated according to the Boltzmann factor that governs the relative populations of the four populated levels. It can be seen that the amplitude of the broadened quadrupole doublet decreases relative to the remainder as the temperature is lowered to 2 K and hence quadrupole doublet must be associated with the *excited* electronic doublet. The broadened doublet can be seen best by taken the difference spectrum "2 K minus 4.2 K", shown in black.

Two conclusions can be drawn from the spectra of Figure S12. First, the presence of a low-lying electronic state (the doublet at $\varepsilon \approx 8J \approx 1.6$ cm^{-1} associated with $d^{EPR\text{-}silent}$) shows that the system is *weakly* exchange coupled. The coupled states (not shown) originating from the $|1^{\pm}>$ levels of Figure S12 are at ≈ 20 cm^{-1} above the ground state and are therefore not populated at the temperatures of Figure S12. Second, the observation that the broadened quadrupole doublet is associated with an electronic excited state shows that $J < 0$.

The 0.3 T spectrum is difficult to simulate, for two reasons. First, for B = 0.3 T the spin expectation value $\langle S_{z1,2} \rangle$ rises steeply (Figure S11) with a slope proportional to $g_z \beta B/\Delta$. A distribution of Δ leads to a distribution of B_{int}, and therefore to broad, unresolved features. Thus, for a correct simulation one needs to know the distribution of Δ (which depends on the distributions of the D_i, $(E/D)_i$ and J).

Within the manifold originating from the four $m_i = \pm 2$ states, the only non-zero matrix elements involve the operators S_{z1}, S_{z2}, implying that our data are only sensitive to J_z. From our combined EPR and Mössbauer study we estimate that $J_z \approx -0.2 \pm 0.1$ cm^{-1}. For such small J values the spin-spin dipolar interactions between the Fe centers may not be negligible. The effective component for this interaction can be written as $\hat{H}_{spin\text{-}dip} = \frac{g_1 g_2 \beta^2}{r^3} (1\text{-}3\cos^2\theta)\hat{S}_{z1}\hat{S}_{z2} = J_{spin\text{-}dip,z}\hat{S}_{z1}\hat{S}_{z2}$, where r is the Fe-Fe distance and θ the angle between the z axis and Fe-Fe direction. We presume that the Fe two sites of diferrous ADO are bridged by carboxylate ligands, but since the bridging mode (μ-(η^1, η^2 and/or μ-1,3, see Wei *et al.*[14]) is not known, the Fe-Fe distance may vary between ≈ 3.3 and 4 Å. Moreover, depending on θ the term may be positive, negative or zero at the magic angle $\theta = 54.74°$. For r = 3.6 Å we have have $J_{spin-dip,z} = 0.038(1 - 3cos^2\theta)$ cm^{-1}. Our analysis depends on $J_{eff,z} = J_z + J_{spin-dip,z}$, and this is the quantity quoted in Table 2 of the main text.

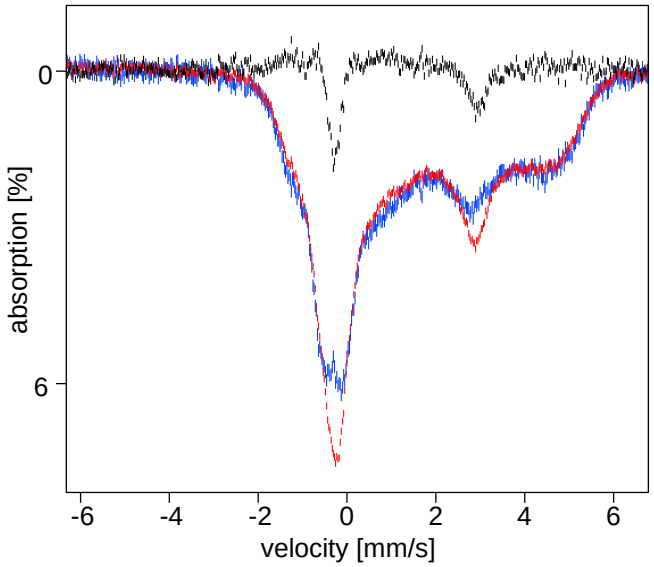

Figure S12. Mössbauer spectra of diferrous ADO recorded at 4.2 K (red) and 2 K (blue) in a parallel applied field of 0.3 T. Above the spectra is shown the difference spectrum "2K minus 4.2 K". This spectrum (sharp low energy line, broadened high energy line) originates from the excited state doublet, roughly $\varepsilon \approx 1.5$ cm^{-1}.

Note on the EPR signal of ADO and MMOH. The integer spin EPR spectra of ADO, observed at X band in parallel and transverse mode, carry much less structural information than the Mössbauer spectra. However, the $g_{eff} \approx 16$ signal of ADO, like the $g_{eff} \approx 16$ feature of MMOH, will be valuable for exploring substrate, inhibitor and dioxygen binding in the diferrous state. We like to comment briefly on two points.

We recently reported a study of MMOH intermediate P* which is generated by reacting diferrous MMOH with dioxygen in the presence of the effector protein MMOB.[15] In this study we observed a decline of the $g_{eff} = 16$ signal after addition of oxygen which seemed to suggest oxidation of the diferrous center. A Mössbauer study, however, revealed that the diiron cluster was still in the diferrous state. The point we wish to make is that minor structure changes of the diferrous state can lead to the disappearance of the $g_{eff} \approx 16$ feature. Recall that the Δ of eq 5 is

given by $\Delta \approx (9/8)\ (E/D)^4 D^2/J$, taken again for simplicity of presentation $D_1 = D_2 = D$ etc. The microwave quantum at X band is $h\nu \approx 0.31$ cm^{-1}. In order to observe the $g_{eff} \approx 16$ signal the quantity Δ has to be smaller than hν. For ADO we found from the EPR simulations an average $\Delta_{avg} \approx 0.31$ cm^{-1} which is distributed by $\sigma_\Delta \approx 0.1$ cm^{-1}(We distributed E/D which yields a somewhat skewed distribution in Δ). Because Δ_{avg} of ADO is (by chance) equal to the microwave quantum at X band, only ≈ 50% of the molecules, namely those having $\Delta < \Delta_{avg}$, contribute to the signal. Also, from the above expression for Δ it can be seen that minor structural changes that lead to small increases of (E/D) and D , or a small decrease of J, can cause the disappearance of the signal. A *decrease* of E/D would keep Δ smaller than hν but easily abolish the resonance as the intensity of the signal is proportional to $\approx (E/D)^8$.

Why $g_{eff} \approx 16$?

We note that the resonance of the weakly coupled system of ADO is observed for $g_{eff} \approx 16$ because the ground doublet exhibits the combined Zeeman splitting of the two sites, which shifts the resonance from $g_{eff} \approx 8$ (of a mononuclear site) to $g_{eff} \approx 16$. The EPR transition observed for diferrous ADO is **not** a transition between $M_S = \pm 4$ states of an $S = 4$ multiplet. Such a multiplet would result in the case of *strong* ferromagnetic exchange, namely for $|J| >> |D_1|, |D_2|$, a condition not even approximately fulfilled for ADO. It is more appropriate here, and for MMOH as well, to refer to $\Delta m_i = 0$ transitions of a weakly coupled system.

REFERENCES

(1) Warui, D. M.; Li, N.; Nørgaard, H.; Krebs, C.; Bollinger, J. M.; Booker, S. J. *J. Am. Chem. Soc.* **2011**, *133*, 3316.

(2) Nash, T. *Biochem. J.* **1953**, *55*, 416.

(3) Numazawa, M.; Yamashita, K.; Kimura, N.; Takahashi, M. *Steroids* **2009**, *74*, 208.
(4) Four, P.; Guibe, F. *J.Org. Chem.* **1981**, *46*, 4439.
(5) Kende, A. S.; Fludzinski, P. *Org. Synth.* **1990**, *Coll. Vol. 7*, 221.
(6) Münck, E.; Surerus, K. K.; Hendrich, M. P. *Methods Enzymol.* **1993**, *227*, 463.
(7) Hendrich, M. P.; Münck, E.; Fox, B. G.; Lipscomb, J. D. *J. Am. Chem. Soc.* **1990**, *112*, 5861.
(8) Hendrich, M. P.; Debrunner, P. G. *Biophys. J.* **1989**, *56*, 489.
(9) Fox, B. G.; Hendrich, M. P.; Surerus, K. K.; Andersson, K. K.; Froland, W. A.; Lipscomb, J. D.; Münck, E. *J. Am. Chem. Soc.* **1993**, *115*, 3688.
(10) Sage, J. T.; Xia, Y. M.; Debrunner, P. G.; Keough, D. T.; De Jersey, J.; Zerner, B. *J. Am. Chem. Soc.* **1989**, *111*, 7239.
(11) Freeman, A. J.; Watson, R. E. *Phys. Rev.* **1962**, *127*, 2058.
(12) Watson, R. E.; Freeman, A. J. *Phys. Rev.* **1964**, *133*, A1571.
(13) Freeman, A. J.; Watson, R. E. In *Magnetism*; Rado, G. T., Suhl, H., Eds.; Academic Press: New York, NY, 1965; Vol. IIA, p 167.
(14) Wei, P.-p.; Skulan, A. J.; Mitić, N.; Yang, Y.-S.; Saleh, L.; Bollinger, J. M.; Solomon, E. I. *J. Am. Chem. Soc.* **2004**, *126*, 3777.
(15) Banerjee, R.; Meier, K. K.; Münck, E.; Lipscomb, J. D. *Biochemistry* **2013**, *52*, 4331.